Research Square

Preprints are preliminary reports that have not undergone peer review.
They should not be considered conclusive, used to inform clinical practice,
or referenced by the media as validated information.

Mathematical Modeling of Lymphatic Filariasis with Quarantine Measures, Treatment Protocols and Drug Resistance in Ghana

Samuel D. Teye
Department of Mathematics, University of Cape Coast
Theophilus Kwofie
Department of Mathematics & Statistics, Austin Peay State University, Clarksville, Tennessee, USA
Samuel Iddi
African Population and Health Research Center, APHRC Campus, Manga Close, Off Kirawa Road, Nairobi, Kenya
Stephen E. Moore
stephen.moore@ucc.edu.gh

Department of Computer Science, University of Pretoria, South Africa

Research Article

Keywords: lymphatic filariasis, quarantine; treatment, resistance dynamics, reproduction number, sensitivity analysis

Posted Date: March 18th, 2026

DOI: https://doi.org/10.21203/rs.3.rs-9149365/v1

License: This work is licensed under a Creative Commons Attribution 4.0 International License.
Read Full License

Additional Declarations: The authors declare no competing interests.

Mathematical Modeling of Lymphatic Filariasis with Quarantine Measures, Treatment Protocols and Drug Resistance in Ghana

Samuel D. Teye[1], Theophilus Kwofie[2,3], Samuel Iddi[4], and Stephen E. Moore*[5]

[1]Department of Mathematics, University of Cape Coast, Cape Coast, Ghana
[2]School of Mathematical and Statistical Sciences, Arizona State University, Tempe, Arizona, USA
[3]Department of Mathematics & Statistics, Austin Peay State University, Clarksville, Tennessee, USA
[4]African Population and Health Research Center, APHRC Campus, Manga Close, Off Kirawa Road, Nairobi, Kenya

Abstract

Lymphatic filariasis (elephantiasis) is a neglected tropical disease caused by parasitic worms that impair the lymphatic system and lead to severe swelling. To better understand its transmission and control, we formulate a deterministic mathematical model to study the transmission dynamics that incorporates treatment, quarantine, and the emergence of drug resistance. The human population is structured into susceptible, exposed, acutely infected, chronically infected, treated, withdrawal, and three resistance stages, while the mosquito population is divided into susceptible, exposed, and infectious classes. The model admits two main equilibrium states: the disease-free equilibrium and the endemic equilibrium. The basic reproduction number, $\mathcal{R}_0$, is derived using the next-generation matrix method. Analytical results show that the disease-free equilibrium is globally asymptotically stable whenever $\mathcal{R}_0 < 1$, while the endemic equilibrium is stable when $\mathcal{R}_0 > 1$. Using Ghana's post-MDA (MAss Drug Administration) surveillance, we estimate four key parameters and three initial conditions. Sensitivity analysis, carried out using Latin Hypercube Sampling and partial rank correlation, identifies the treatment rate, resistance progression, and mosquito biting rate as the most influential factors affecting transmission. Numerical simulations further demonstrate that treatment alone achieves a greater reduction in prevalence compared to quarantine alone, while a combined intervention of treatment and quarantine yields the most significant impact. These findings suggest that integrated control strategies, particularly those accounting for drug resistance, are vital for the effective and sustainable management of lymphatic filariasis.

Keywords: lymphatic filariasis; quarantine; treatment; resistance dynamics; reproduction number; sensitivity analysis.

1 Introduction

Lymphatic filariasis, also known as elephantiasis, is an overlooked tropical condition that significantly damages the economic and social systems in Asia, Africa, the Western Pacific, and certain regions in the United States [16]. It is the leading cause of persistent and permanent disability [25]. Globally, the disease affects approximately 120 million people with about 36 million suffering from severe incapacity or disfigurement. It is one of the most common and underrecognized tropical diseases, carrying significant socioeconomic burden [14, 1]. Lymphatic filariasis can affect people across all age groups, impacting men, women and children alike. The disease is triggered by tissue-dwelling nematodes, especially Brugia malayi, Brugia timori, and Wuchereria bancrofti [24]. Elephantiasis is a pathogenic illness created by thread-shaped worms that affects around 1.4 billion people in 73 countries around the world [25]. In males, lymphatic filariasis may lead to chronic complications including lymphedema, elephantiasis, and hydrocele and is transmitted between individuals through mosquito vectors. Lymphatic filariasis is an important issue for the public in the African continent, South America, and Asia, despite a global treatment effort and a solid understanding of the disease's pathogenesis [25]. Microfilariae and some adult worms can be killed with drugs such as Diethylcarbamazine plus Albendazole and Ivermectin plus Albendazole. However, there is insufficient data to support Albendazole's efficacy, either by itself or in combination, in killing or preventing the spread of the worms which trigger elephantiasis [4]. Some research suggest that Doxycycline has the potential to totally eradicate microfilariae [5].

The eradication of this disease remains a big challenge, necessitating the need for evaluations of integrated intervention strategies such as mass treatment and clinical management of chronic cases through quarantine. Quarantining such individuals

*corresponding author: stephen.moore@ucc.edu.gh

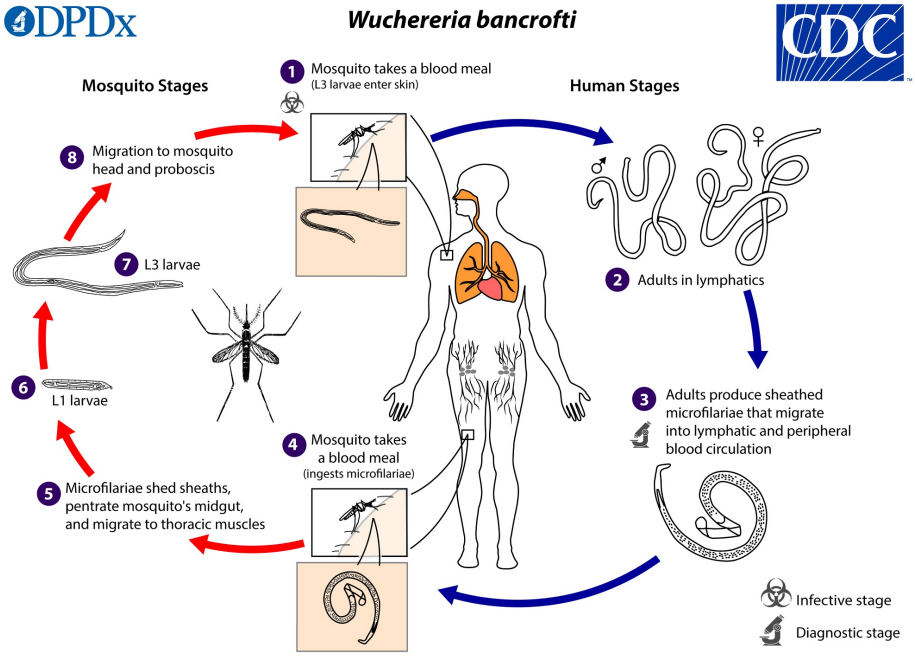


Figure 1: Life cycle of the roundworm that causes lymphatic filariasis (LF). Source: Centers for Disease Control and Prevention (CDC), DPDx. Available at: https://www.cdc.gov/dpdx/lymphaticfilariasis/index.html.

may help to prevent the propagation of the infection [22, 25]. Bed nets treated with insecticide (ITNs) and the use of indoor residual spraying (IRS) might limit interaction between people (particularly microfilariae carriers) and vectors of mosquitoes [16]. Despite uncertainty over the microfilarial prevalence threshold required to sustain transmission in the absence of medicines, therapy remains the primary means of protection against the illness [25].

Several compartmental mathematical frameworks for lymphatic filariasis are available within the scientific literature, the deterministic model based on population EPIFIL and the stochastic model based on individuals (LYMFASIM) are two significant simulation models used to enhance decision-making in the spread and management of lymphatic filariasis . However, these models exclude intervention approaches such as quarantine,which presents a limitation. EPIFIL employs a continual force of infection and takes into account the effect on the people and neighborhood's age structure , whereas LYMFASIM examines the role of the immune system in parasite control [20].

[10] stated that mathematical modeling can help maximize the use of limited resources by analyzing the spread patterns and the economic viability of diseases that are neglected, whereas [16] provided tools and techniques to manage lymphatic filariasis transmission and morbidity. The compartmental model proposed by [15], although useful in providing insight into the transmission dynamics of lymphatic filariasis, is not comprehensive and has notable limitations. In particular, it fails to account for parasite prevalence that varies with density and species. According to [9], an increase in mosquito infection intensity may be connected with density-dependent mosquito death. Furthermore, mass pharmaceutical delivery may raise mosquito survival rates, potentially leading to a long-term increase transmission [9].

Resistance to antihelminthics, commonly used to treat human infections, is a major concern [7]. It has already been reported that the widespread use of benzimidazoles (BZ) and the use of Ivermectin (IVM) in human medicine has led to the emergence of drug-resistant strains. [17].

Given this, it is reasonable to expect that mass drug administration (MDA) in large population groups over several years might impose a substantial selective stress on parasitic organisms, likely contributing to the evolution of resistance to medication types [8]. As the size of the population groups and the duration of the program expand, the danger of treatment failure due to the establishment of resistance becomes increasingly obvious. Furthermore, filarial parasite genetic variation may have a substantial impact on medication efficacy as well as the establishment and dissemination of resistance [18].

So far, there has been evidence of non-susceptibility to DEC in filarial worms [6], but complete resistance studies are difficult due to an absence of comprehension regarding its mode of action. [13] found Onchocerca volvulus to be resistant to IVM but no resistance in Wuchereria bancrofti has been proven. However, numerous nematode parasites are showing resistance to BZ [19]. Despite these discoveries, the importance and mechanisms of medication resistance remain unclear. To determine the amount of antihelminthic resistance in elephantiasis and identifying the key factors contributing to parasite drug resistance, gaining such insight will enhance our understanding of potential treatment failures associated with mass drug administration.

Despite extensive research into the mechanics of lymphatic filariasis transmission, there is still a significant vacuum in our understanding of drug resistance. This study tries to address these shortcomings by constructing a Susceptible, Exposed, Infected, Susceptible (SEIS) mathematical model that incorporates drug resistance, determines the basic reproduction number, executes numerical simulations of the model, and assesses both local and global stability.

The rest of the article is organized as follows: In Section 2, we present the mathematical model formulation, including the compartments, assumptions, and governing differential equations. Section 3 provides the analysis of the model, such as positivity, boundedness, and stability of equilibria, together with the computation of the basic reproduction number. In Section 4, we describe parameter estimation using Ghana's post-MDA surveillance data. Section 6 contains the numerical simulations and sensitivity analysis to explore intervention strategies. Finally, Section 7 concludes the article with key findings and policy implications.

2 Mathematical Model Formulation

The model is structured into twelve compartments, dividing the population into different classes. Both the human and mosquito populations are categorized based on their lymphatic filariasis status. The human population is subdivided into the following compartments: susceptible individuals, $S_h(t)$, exposed individuals, $E_h(t)$, acute infected individuals, $I_{ha}(t)$, chronically infected individuals, $I_{hc}(t)$, treated acute infected individuals, $T_h(t)$and withdrawal of treated individuals, $W_h(t)$ representing individuals who have completed treatment successfully and are temporarily withdrawn from the treatment compartment. They may eventually lose protection and return to the susceptible class at a rate ρ, $R_1(t)$ First-stage drug resistance, representing individuals who after treatment retain partial worm survival leading to reduced treatment efficacy, $R_2(t)$ Second-stage drug resistance, representing individuals who have progressed to a higher level of resistance due to repeated treatment failure or parasite adaptation, $R_3(t)$ Third-stage (advanced) drug resistance, representing individuals where the parasites are highly tolerant to treatment, making conventional drugs ineffective . The total human population is given by:

$$\begin{aligned} N_h(t) = S_h(t) + E_h(t) + I_{ha}(t) + I_{hc}(t) + T_h(t) \\ + W_h(t) + R_1(t) + R_2(t) + R_3(t). \end{aligned} \tag{2.1}$$

This model is predicated on the idea that there isn't an infection in the beginning. Additionally, we presume that individuals in the infected-acute and infected-chronic populations transmit the infection to the mosquito population, regardless of various quarantine measures applied to infected-chronic individuals. The mosquito population is divided into three compartments: susceptible mosquitoes, $S_m(t)$, exposed mosquitoes, $E_m(t)$, and infected mosquitoes, $I_m(t)$. The total mosquito population is expressed as

$$N_m(t) = S_m(t) + E_m(t) + I_m(t). \tag{2.2}$$

The recruitment rate of the human population is denoted by Λ_h, while Λ_m represents the recruitment rate of the mosquito population. The natural death rates for the human and mosquito populations are μ_h and μ_m, respectively. The symbol for the mosquito bite rate on humans is β. Susceptible mosquitoes are infected by microfilariae, which live in the lymphatic nodes and channels, when they bite individuals in the infected-acute or infected-chronic stage during a blood meal [21]. This occurs at a rate given by

$$\lambda_m(t) = \frac{\beta\vartheta_m(I_{ha}(t) + \delta I_{hc}(t))}{N_h(t)}. \tag{2.3}$$

The vector ingests microfilariae at various rates when it bites humans in the infected-acute stage, $I_{ha}(t)$, and the infected-chronic stage, $I_{hc}(t)$. The rate at which microfilariae are discharged is $\vartheta_m\delta$ from individuals in $I_{ha}(t)$. Once consumed, the sensitive mosquito transfers into the exposed class, $E_m(t)$. The microfilariae transform into infectious filariform larvae at this stage. The mosquito then advances into the infected class, $I_m(t)$, at a pace α_m. The rate at which the larvae infect a susceptible human host during a subsequent intake of blood by the infected mosquito is determined by:

$$\lambda_h(t) = \frac{\beta\vartheta_h I_m(t)}{N_h(t)}. \tag{2.4}$$

Using the descriptions, assumptions, and definitions of state variables. We derive the following nonlinear system of ordinary differential equations that characterizes the proposed SEIS model for lymphatic filariasis.

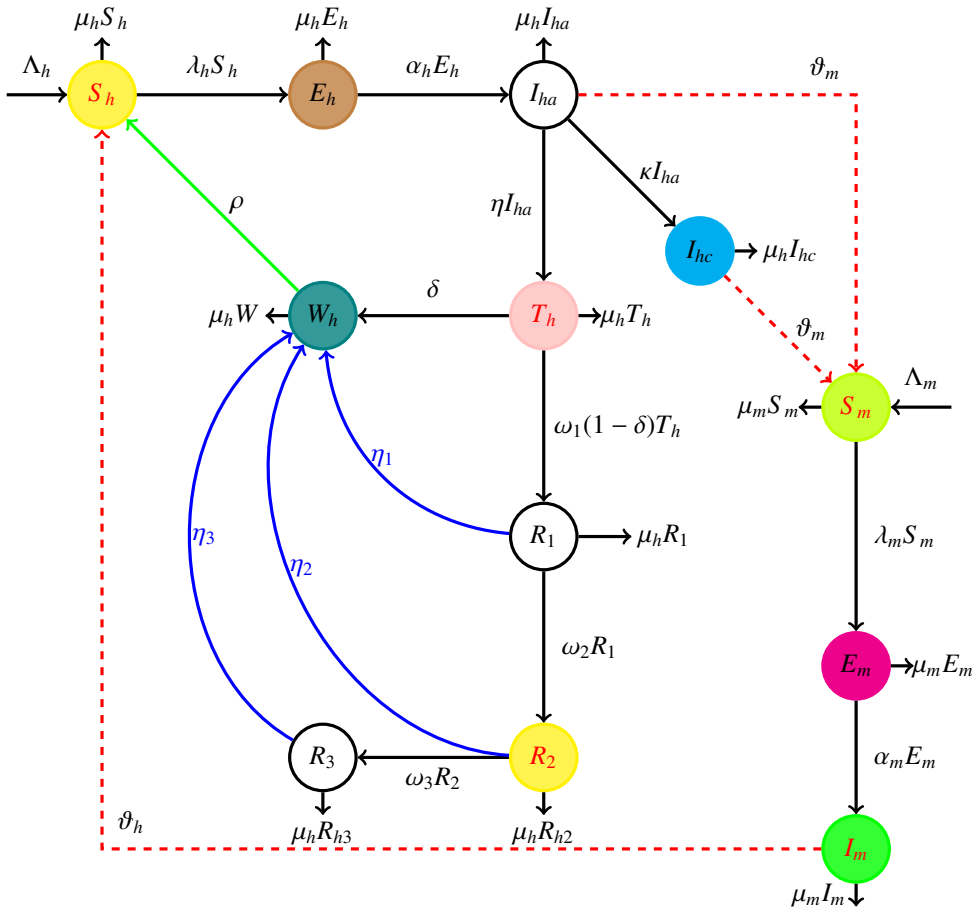


Figure 2: Flow diagram for the transmission dynamics of lymphatic filariasis

Table 2: Model parameter descriptions and their units (Table 3 provides the values used in simulations).

Parameter	**Description**	**Unit**
Λ_h	Recruitment rate of humans	individuals/day
Λ_m	Recruitment rate of mosquitoes	mosquitoes/day
μ_h	Natural death rate of humans	1/day
μ_m	Natural death rate of mosquitoes	1/day
β	Mosquito biting rate on humans	bites/mosquito/day
ϑ_h	Transmission probability from mosquito to human	dimensionless
ϑ_m	Transmission probability from human to mosquito	dimensionless

Table 1: State variable description

State Variables	**Description**
S_h	Susceptible humans
E_h	Exposed humans
I_{ha}	Infected-acute humans
I_{hc}	Quarantined Infected chronic humans
T_h	Treatment of infected-acute
W_h	Withdrawal of treated humans
R_1, R_2, R_3	Resistance to drug
S_m	Susceptible mosquitoes
E_m	Exposed mosquitoes
I_m	Infected mosquitoes

κ	Rate of progression from acute to chronic infection in humans	1/day
η	Chemotherapy/ treatment rate of acutely infected humans	1/day
η_1, η_2, η_3	Immunity development rates for resistance classes	1/day
$\omega_1, \omega_2, \omega_3$	Progression rates between resistance classes	1/day
ρ	Rate of loss of partial immunity	1/day
α_h	Rate of progression from exposed to acutely infected humans	1/day
α_m	Rate of progression from exposed to infected mosquitoes	1/day
δ	The rate at which individual acquired partial immunity	dimensionless

Using the stated assumptions and flow diagram, we derive the following nonlinear ODE system.

$$\begin{cases} \frac{dS_h}{dt} = \Lambda_h + \rho W_h - \frac{\beta\vartheta_h I_m S_h}{N_h} - \mu_h S_h \\ \frac{dE_h}{dt} = \frac{\beta\vartheta_h I_m S_h}{N_h} - (\alpha_h + \mu_h)E_h \\ \frac{dI_{ha}}{dt} = \alpha_h E_h - \eta I_{ha} - (\kappa + \mu_h)I_{ha} \\ \frac{dI_{hc}}{dt} = \kappa I_{ha} - \mu_h I_{hc} \\ \frac{dT_h}{dt} = \eta I_{ha} - (\delta + \omega_1(1-\delta) + \mu_h)T_h \\ \frac{dW_h}{dt} = \delta T_h + \eta_1 R_1 + \eta_2 R_2 + \eta_3 R_3 - (\rho + \mu_h)W_h \\ \frac{dR_1}{dt} = \omega_1(1-\delta)T_h - (\omega_2 + \eta_1 + \mu_h)R_1 \\ \frac{dR_2}{dt} = \omega_2 R_1 - (\omega_3 + \eta_2 + \mu_h)R_2 \\ \frac{dR_3}{dt} = \omega_3 R_2 - (\eta_3 + \mu_h)R_3 \\ \frac{dS_m}{dt} = \Lambda_m - \frac{\beta\vartheta_m(I_{ha} + \delta I_{hc})S_m}{N_m} - \mu_m S_m \\ \frac{dE_m}{dt} = \frac{\beta\vartheta_m(I_{ha} + \delta I_{hc})S_m}{N_h} - (\alpha_m + \mu_m)E_m \\ \frac{dI_m}{dt} = \alpha_m E_m - \mu_m I_m \end{cases} . \tag{2.5}$$

From the model diagram in Figure 2. The non-linear ordinary differential equations that describe the transmission dynamics of lymphatic filariasis With the following initial conditions: $S_h(0) > 0, E_h(0) \geqslant 0, I_{ha}(0) \geqslant 0, I_{hc}(0) \geqslant 0, T_h(0) \geqslant 0, W_h(0) \geqslant 0, R_1(0) \geqslant 0, R_2(0) \geqslant 0, R_3(0) \geqslant 0, S_m(0) > 0, E_m(0) \geqslant 0, I_m(0) \geqslant 0$.

3 Analysis of Lymphatic Filariasis Model

This section presents the analysis of the lymphatic filariasis transmission of model (2.5) to establish its mathematical and biological validity and to explore its long-term behavior. The analysis focuses on determining the conditions under which the disease either dies out or becomes endemic, based on the basic reproduction number, $\mathcal{R}_0$. It can be shown that the model (2.5) solutions remain non-negative and bounded within a biologically feasible region. The stability of the disease-free and endemic equilibria is then examined, as these equilibria govern the ultimate outcome of the infection dynamics.

3.1 Positivity of Solutions

Model (2.5) monitors the human population, so it is crucial that all state variables remain non-negative. Therefore, the solutions to model (2.5) must remain non-negative for $t \geq 0$. To ensure this, the following theorem is applied.

Theorem 3.1. *Consider the SEIR model system 2.5 with non-negative initial conditions:*

$$\{S_h(0),\ E_h(0),\ I_{ha}(0),\ I_{hc}(0),\ T_h(0),\ W_h(0), R_1(0),\ R_2(0),\ R_3(0),\ S_m(0),\ E_m(0),\ I_m(0)\} \geq 0.$$

Then, the solution remains in $\mathbb{R}^{12}_+$ *for all* $t \geq 0$*, for every* $t \in [0, T]$.

Proof. We show that all state variables remain nonnegative for all $t \geq 0$, given nonnegative initial conditions. We present the argument for $S_h(t)$; the remaining compartments, which follow similarly.

From (2.5) we consider the equation for $S_h(t)$:

$$\frac{dS_h}{dt} = \Lambda_h + W_h - \lambda_h(t)\, S_h - \mu_h S_h,$$

it follows that

$$\frac{dS_h}{dt} \geq -(\lambda_h(t) + \mu_h)\, S_h,$$

dividing by $S_h > 0$ and integrating from 0 to t gives

$$\int_{S_h(0)}^{S_h(t)} \frac{dS_h}{S_h} \geq -\int_0^t (\lambda_h(s) + \mu_h)\, ds,$$

this yields

$$\ln S_h(t) - \ln S_h(0) \geq -\int_0^t (\lambda_h(s) + \mu_h)\, ds,$$

hence

$$S_h(t) \geq S_h(0) \exp\Big(-\int_0^t (\lambda_h(s) + \mu_h)\, ds\Big) \geq 0.$$

Thus, all state variables remain nonnegative for all $t \geq 0$. Therefore, it $S_h(t)$ is positive for $t > 0$.

Similarly, it can be shown that, $E_h(t) \geq 0, I_{ha}(t) \geq 0, I_{hc}(t) \geq 0, T_h(t) \geq 0, W_h(t) \geq 0, R_1(t) \geq 0, R_2(t) \geq 0, R_3(t) \geq 0, S_m(t) > 0, E_m(t) \geq 0, I_m(t) \geq 0$. □

3.2 Invariant Region

To ensure biological realism, we consider all parameters and state variables to remain non-negative for every $t \geq 0$. Suppose the solution vector evolves from an initial condition with non-negative values. The following sets represent the biologically feasible regions for the human and mosquito populations, respectively:

Theorem 3.2. *The solutions of model (2.5) are contained in the region $\Omega \subset \mathbb{R}^{12}_+$, where Ω represents the set of all biologically feasible solutions for the human and mosquito populations.*

Proof. The feasible region for the human population is defined as:

$$\Omega_h = \left\{(S_h, E_h, I_{ha}, I_{hc}, T_h, W_h, R_1, R_2, R_3) : N_h(t) \leq \frac{\Lambda_h}{\mu_h}\right\}. \tag{3.1}$$

Similarly, the feasible region for the mosquito population is given by:

$$\Omega_m = \left\{(S_m, E_m, I_m) : N_m(t) \leq \frac{\Lambda_m}{\mu_m}\right\}. \tag{3.2}$$

By employing the differential inequality result established by [3], it follows that as $t \to \infty$, the human population $N_h(t)$ satisfies

$$N_h'(t) < \Lambda_h - \mu_h N_h(t).$$

Consequently, $N_h(t)$ is confined within the bounds

$$0 \leq N_h(t) \leq \frac{\Lambda_h}{\mu_h}.$$

Therefore, the human population trajectories are restricted to the positively invariant region Ω_h, and similarly, the mosquito population remains within Ω_m. □

Basic Reproduction Number

The basic reproduction number, $\mathcal{R}_0$, is determined using the next-generation matrix method [23], where $\mathcal{R}_0 = \rho(FV^{-1})$, with F and V denote the new infection and transition matrices, respectively.

We let

$$\mathbf{F} = \begin{pmatrix} \frac{\beta\vartheta_h I_m S_h}{N_h} \\ 0 \\ 0 \\ 0 \\ 0 \\ 0 \\ 0 \\ 0 \\ \frac{\beta\vartheta_m (I_{ha}+\delta I_{hc}) S_m}{N_h} \\ 0 \end{pmatrix}$$

and

$$\mathbf{V} = \begin{pmatrix} \Gamma_1 & 0 & 0 & 0 & 0 & 0 & 0 & 0 & 0 & 0 \\ -\alpha_h & \Gamma_2 & 0 & 0 & 0 & 0 & 0 & 0 & 0 & 0 \\ 0 & -\kappa & \Gamma_3 & 0 & 0 & 0 & 0 & 0 & 0 & 0 \\ 0 & -\eta & 0 & \Gamma_4 & 0 & 0 & 0 & 0 & 0 & 0 \\ 0 & 0 & 0 & -\delta & \Gamma_5 & -\eta_1 & -\eta_2 & -\eta_3 & 0 & 0 \\ 0 & 0 & 0 & (\delta-1)\omega_1 & 0 & \Gamma_6 & 0 & 0 & 0 & 0 \\ 0 & 0 & 0 & 0 & 0 & -\omega_2 & \Gamma_7 & 0 & 0 & 0 \\ 0 & 0 & 0 & 0 & 0 & 0 & -\omega_3 & \Gamma_8 & 0 & 0 \\ 0 & 0 & 0 & 0 & 0 & 0 & 0 & 0 & \Gamma_9 & 0 \\ 0 & 0 & 0 & 0 & 0 & 0 & 0 & 0 & -\alpha_m & \Gamma_{10} \end{pmatrix} \tag{3.3}$$

where, $\Gamma_1 = (\alpha_h + \mu_h), \Gamma_2 = (\eta + \kappa + \mu_h), \Gamma_3 = \mu_h, \Gamma_4 = -(\delta-1)\omega_1 + \delta + \mu_h, \Gamma_5 = (\rho + \mu_h), \Gamma_6 = (\omega_2 + \eta_1 + \mu_h), \Gamma_7 = (\omega_3 + \eta_2 + \mu_h), \Gamma_8 = (\eta_3 + \mu_h), \Gamma_9 = (\alpha_m + \mu_h), \Gamma_{10} = \mu_m$.

The basic reproduction number $\mathcal{R}_0$ is a spectral radius, $\rho(FV^{-1})$ and the result is given by

$$\mathcal{R}_0 = \frac{\sqrt{\frac{(\delta\kappa + \mu_h)\vartheta_h\vartheta_m\Lambda_m\alpha_h\alpha_m}{\left(\alpha_h\eta + \alpha_h\kappa + (\alpha_h + \eta + \kappa)\mu_h + \mu_h^2\right)\Lambda_h(\alpha_m + \mu_m)}}\beta}{\mu_m}.$$

3.3 Disease-Free Equilibrium and Stability Analysis

The disease-free equilibrium E_0 is a state where no individual is infected or transmitting the disease, given by:

$$E_0 = \left(\frac{\Lambda_h}{\mu_h}, 0, 0, 0, 0, 0, 0, 0, 0, \frac{\Lambda_m}{\mu_m}, 0, 0\right),$$

where the components correspond to $(S_h, E_h, I_{ha}, I_{hc}, T_h, R_1, R_2, R_3, W_h, S_m, E_m, I_m)$, respectively.

3.3.1 Local stability of the disease-free equilibrium

Lemma 3.1. *The DFE for the lymphatic filariasis model (2.5) is locally asymptotically stable if $\mathcal{R}_0 < 1$ and unstable when $\mathcal{R}_0 > 1$.*

Proof. The Routh-Hurwitz criterion is employed to analyze the local stability of model 2.5 by evaluating the Jacobian matrix at the disease-free equilibrium (DFE) as shown below:

$$\mathbf{V} = \begin{pmatrix} \Gamma_1 - \lambda & 0 & 0 & 0 & 0 & 0 & 0 & 0 & 0 & 0 \\ -\alpha_h & \Gamma_2 - \lambda & 0 & 0 & 0 & 0 & 0 & 0 & 0 & 0 \\ 0 & -\kappa & \Gamma_3 - \lambda & 0 & 0 & 0 & 0 & 0 & 0 & 0 \\ 0 & -\eta & 0 & \Gamma_4 - \lambda & 0 & 0 & 0 & 0 & 0 & 0 \\ 0 & 0 & 0 & -\delta & \Gamma_5 - \lambda & -\eta_1 & -\eta_2 & -\eta_3 & 0 & 0 \\ 0 & 0 & 0 & (\delta - 1)\omega_1 & 0 & \Gamma_6 - \lambda & 0 & 0 & 0 & 0 \\ 0 & 0 & 0 & 0 & 0 & -\omega_2 & \Gamma_7 - \lambda & 0 & 0 & 0 \\ 0 & 0 & 0 & 0 & 0 & 0 & -\omega_3 & \Gamma_8 - \lambda & 0 & 0 \\ 0 & 0 & 0 & 0 & 0 & 0 & 0 & 0 & \Gamma_9 - \lambda & 0 \\ 0 & 0 & 0 & 0 & 0 & 0 & 0 & 0 & -\alpha_m & \Gamma_{10} - \lambda \end{pmatrix} \tag{3.4}$$

where, $\Gamma_1 = (\alpha_h + \mu_h), \Gamma_2 = (\eta + \kappa + \mu_h), \Gamma_3 = \mu_h, \Gamma_4 = -(\delta - 1)\omega_1 + \delta + \mu_h, \Gamma_5 = (\rho + \mu_h), \Gamma_6 = (\omega_2 + \eta_1 + \mu_h), \Gamma_7 = (\omega_3 + \eta_2 + \mu_h), \Gamma_8 = (\eta_3 + \mu_h), \Gamma_9 = (\alpha_m + \mu_h), \Gamma_{10} = \mu_m$.

The following characteristics polynomials are obtained:

$$0 = -(\alpha_h + \mu_h) - \lambda \tag{3.5}$$

$$0 = -\delta\eta\lambda - \delta\eta\mu_h + \eta\lambda + \eta\mu_h + \kappa\lambda + \kappa\mu_h + \lambda^2 + 2\lambda\mu_h + \mu_h^2, \tag{3.6}$$

$$0 = \lambda^2 + 2\lambda\mu_h + \lambda\omega_1 + \lambda\phi + \lambda\rho + \mu_h^2 + \mu_h\omega_1 + \mu_h\phi + \mu_h\rho + \omega_1\rho + \phi\rho, \tag{3.7}$$

$$0 = \alpha_m\lambda + \alpha_m\mu_m + \lambda^2 + \lambda\mu_h + \lambda\mu_m + \mu_h\mu_m \tag{3.8}$$

$$\begin{aligned} 0 = {} & -\eta_1\eta_2\eta_3 - \eta_1\eta_2\lambda - \eta_1\eta_2\mu_h - \eta_1\eta_3\lambda - \eta_1\eta_3\mu_h - \eta_1\eta_3\omega_3 - \eta_1\lambda^2 - 2\eta_1\lambda\mu_h - \eta_1\lambda\omega_3 - \eta_1\mu_h^2 - \eta_1\mu_h\omega_3 \\ & - \eta_2\eta_3\lambda - \eta_2\eta_3\mu_h - \eta_2\eta_3\omega_2 - \eta_2\lambda^2 - 2\eta_2\lambda\mu_h - \eta_2\lambda\omega_2 - \eta_2\mu_h^2 - \eta_2\mu_h\omega_2 - \eta_3\lambda^2 \\ & - 2\eta_3\lambda\mu_h - \eta_3\lambda\omega_2 - \eta_3\lambda\omega_3 - \eta_3\mu_h^2 - \eta_3\mu_h\omega_2 - \eta_3\mu_h\omega_3 - \eta_3\omega_2\omega_3 - \lambda^3 \\ & - 3\lambda^2\mu_h - \lambda^2\omega_2 - \lambda^2\omega_3 - 3\lambda\mu_h^2 - 2\lambda\mu_h\omega_2 - 2\lambda\mu_h\omega_3 - \lambda\omega_2\omega_3 - \mu_h^3 - \mu_h^2\omega_2 - \mu_h^2\omega_3 - \mu_h\omega_2\omega_3. \end{aligned} \tag{3.9}$$

From the characteristic polynomials, it is easy to see that the eigenvalues are negative. □

3.3.2 Global stability of the disease-free equilibrium

With all state variables shown to remain nonnegative for $t \geq 0$, we now examine the long-term behavior of the system at the disease-free equilibrium (DFE), where no infection persists. Positivity and boundedness ensure the variables remain biologically meaningful, forming the basis for stability analysis. We aim to prove that the DFE is globally asymptotically stable when the basic reproduction number $\mathcal{R}_0 < 1$, using Lyapunov functions to demonstrate that the disease will ultimately be eradicated regardless of initial conditions.

Lemma 3.2. *The DFE of model (2.5) is globally asymptotically stable if $\mathcal{R}_0 < 1$ and unstable when $\mathcal{R}_0 > 1$.*

Proof. The system of equations (2.5) can be divided into two subsystems:

$$X_1 = (S_h, S_m), \quad \text{representing the susceptible compartments of humans and mosquitoes,}$$

$Y_1 = (E_h, I_{ha}, I_{hc}, T_h, W_h, R_1, R_2, R_3, E_m, I_m)$, representing the exposed, infected, treated, and recovered compartments accordingly, the model (2.5) can be rewritten in the reduced form:

$$\begin{cases} \dfrac{dX_1}{dt} = F(X_1, Y_1), \\ \dfrac{dY_1}{dt} = G(X_1, Y_1) \end{cases} \quad \text{where} \quad X_1 \in \mathbb{R}_+^2,\ Y_1 \in \mathbb{R}_+^{10} \tag{3.10}$$

Further simplification by identifying X_1 with $(X_1, 0)$ and Y_1 with $(0, Y_1)$ in $\mathbb{R}_+^2 \times \mathbb{R}_+^{10}$. The reduced system is obtained as $\dfrac{dX_1}{dt} = F(X_1, 0)$ follows:

$$\begin{cases} \dfrac{dS_h}{dt} = \Lambda_h - \mu_h S_h, \\ \dfrac{dS_m}{dt} = \Lambda_m - \mu_m S_m. \end{cases} \tag{3.11}$$

However, there

$$X_1^* = (S_h^*, S_m^*) = \left(\frac{\Lambda_h}{\mu_h}, \frac{\Lambda_m}{\mu_m}\right)$$

is a globally asymptotically stable equilibrium for the reduced system

$$\frac{dX_1}{dt} = F(X_1, 0).$$

This is verified by integrating the first equation of the reduced system 3.11 from 0 to t. We obtain

$$S_h(t) = \frac{\Lambda_h}{\mu_h} + \left(S_h(0) - \frac{\Lambda_h}{\mu_h}\right)e^{-\mu_h t},$$

which approaches $\frac{\Lambda_h}{\mu_h}$ as $t \to \infty$. Similarly, integrating the second equation of the reduced system 3.11 from 0 to t gives

$$S_m(t) = \frac{\Lambda_m}{\mu_m} + \left(S_m(0) - \frac{\Lambda_m}{\mu_m}\right)e^{-\mu_m t},$$

which approaches $\frac{\Lambda_m}{\mu_m}$ as $t \to \infty$. In addition, it $G(X_1, Y_1)$ applies to the two criteria in [11] thus $G(X_1, 0) = 0$ and $G(X_1, Y_1) = A_1^* Y_1 - \hat{G}(X_1, Y_1)$ where $\hat{G}(X_1, Y_1) \geq 0$ the system of differential equation 2.5 is written as,

$$\begin{cases} \frac{dX_1}{dt} = F(X_1, Y_1) \\ \frac{dY_1}{dt} = G(X_1, Y_1) \end{cases} \tag{3.12}$$

These criteria are created as,

- Scenario $[T_1]$: For $\frac{dX_1}{dt} = F(X_1, 0)$, X_1^* is globally asymptotically stable.
- Scenario $[T_2]$: $G(X_1, Y_1) = A_1 Y_1 - \hat{G}(X_1, Y_1)$ with $G(X_1, Y_1) \geq 0$ for $(X_1, Y_1) \geq 0$,

where $A_1 = DY_1 G(X_1^*, 0)$ is an (M-matrix). Using the properties of the M-matrix, the disease-free equilibrium (DFE) of the lymphatic filariasis model, denoted by E_0, is globally asymptotically stable provided that the basic reproduction number $\mathcal{R}_0 < 1$ and conditions T_1 ,T_2 hold. □

Theorem 3.3. *Then the lymphatic filariasis at disease-free equilibrium is globally asymptotically stable if $\mathcal{R}_0 < 1$ and only if the scenario T_1 and T_2 are satisfied.*

Proof. We therefore focus on the infected subsystem $(E_h, I_{ha}, I_{hc}, T_h, W_h, R_1, R_2, R_3, E_m, I_m)$ as defined in (3.12).

$$Y_1 = \begin{pmatrix} \beta\vartheta_h I_m S_h/N_h - (\alpha_h + \mu_h)E_h, \\ \alpha_h E_h - \eta(\delta - 1)I_{ha} - (\kappa + \mu_h)I_{ha}, \\ \kappa I_{ha} - \mu_h I_{hc}, \\ \eta(\delta - 1)I_{ha} - (\phi + \omega_1 + \mu_h)T_h, \\ \phi T_h + \eta_1 R_1 + \eta_2 R_2 + \eta_3 R_3 - (\rho + \mu_h)W_h, \\ \omega_1 T_h - (\omega_2 + \eta_1 + \mu_h)R_1, \\ \omega_2 R_1 - (\omega_3 + \eta_2 + \mu_h)R_2, \\ \omega_3 R_2 - (\eta_3 + \mu_h)R_3, \\ \beta\vartheta_m(I_{ha} + \delta I_{hc})S_m/N_m - (\alpha_m + \mu_m)E_m, \\ \alpha_m E_m - \mu_m I_m. \end{pmatrix} \tag{3.13}$$

Equation (3.13) can be represented in matrix form as follows:

$$Y_1' = \begin{pmatrix} -\Gamma_1 & 0 & 0 & 0 & 0 & 0 & 0 & 0 & 0 & 0 \\ \alpha_h & -\Gamma_2 & 0 & 0 & 0 & 0 & 0 & 0 & 0 & 0 \\ 0 & \kappa & -\Gamma_3 & 0 & 0 & 0 & 0 & 0 & 0 & 0 \\ 0 & \eta & 0 & -\Gamma_4 & 0 & 0 & 0 & 0 & 0 & 0 \\ 0 & 0 & 0 & \delta & -\Gamma_5 & \eta_1 & \eta_2 & \eta_3 & 0 & 0 \\ 0 & 0 & 0 & \omega_1(1-\delta) & 0 & -\Gamma_6 & 0 & 0 & 0 & 0 \\ 0 & 0 & 0 & 0 & 0 & \omega_2 & -\Gamma_7 & 0 & 0 & 0 \\ 0 & 0 & 0 & 0 & 0 & 0 & \omega_3 & -\Gamma_8 & 0 & 0 \\ 0 & 0 & 0 & 0 & 0 & 0 & 0 & 0 & -\Gamma_9 & 0 \\ 0 & 0 & 0 & 0 & 0 & 0 & 0 & 0 & \alpha_m & -\Gamma_{10} \end{pmatrix} \begin{pmatrix} E_h \\ I_{ha} \\ I_{hc} \\ T_h \\ W_h \\ R_1 \\ R_2 \\ R_3 \\ E_m \\ I_m \end{pmatrix} - \begin{pmatrix} \beta\vartheta_h I_m \left(1 - \frac{S_h}{N_h}\right) \\ 0 \\ 0 \\ 0 \\ 0 \\ 0 \\ 0 \\ 0 \\ \beta\vartheta_m (I_{ha} + \delta I_{hc}) \left(\frac{\Lambda_m \mu_h}{\mu_m \Lambda_h} - \frac{S_m}{N_h}\right) \\ 0 \end{pmatrix} \tag{3.14}$$

which is in the form $Y_1' = A_1 Y_1 - \hat{G}(X_1, Y_1)$, as in condition T_2 we have,

$$A_1 = \begin{pmatrix} -\Gamma_1 & 0 & 0 & 0 & 0 & 0 & 0 & 0 & 0 & 0 \\ \alpha_h & -\Gamma_2 & 0 & 0 & 0 & 0 & 0 & 0 & 0 & 0 \\ 0 & \kappa & -\Gamma_3 & 0 & 0 & 0 & 0 & 0 & 0 & 0 \\ 0 & \eta & 0 & -\Gamma_4 & 0 & 0 & 0 & 0 & 0 & 0 \\ 0 & 0 & 0 & \delta & -\Gamma_5 & \eta_1 & \eta_2 & \eta_3 & 0 & 0 \\ 0 & 0 & 0 & \omega_1(1-\delta) & 0 & -\Gamma_6 & 0 & 0 & 0 & 0 \\ 0 & 0 & 0 & 0 & 0 & \omega_2 & -\Gamma_7 & 0 & 0 & 0 \\ 0 & 0 & 0 & 0 & 0 & 0 & \omega_3 & -\Gamma_8 & 0 & 0 \\ 0 & 0 & 0 & 0 & 0 & 0 & 0 & 0 & -\Gamma_9 & 0 \\ 0 & 0 & 0 & 0 & 0 & 0 & 0 & 0 & \alpha_m & -\Gamma_{10} \end{pmatrix}$$

and

$$\hat{G}(X_1, Y_1) = \begin{pmatrix} \beta\vartheta_h I_m \left(1 - \frac{S_h}{N_h}\right) \\ 0 \\ 0 \\ 0 \\ 0 \\ 0 \\ 0 \\ 0 \\ \beta\vartheta_m (I_{ha} + \delta I_{hc}) \left(\frac{\Lambda_m \mu_h}{\mu_m \Lambda_h} - \frac{S_m}{N_h}\right) \\ 0 \end{pmatrix}$$

where, $N_h = \dfrac{\Lambda_h}{\mu_h}$ is the total human population and $N_m = \frac{\Lambda_m}{\mu_m}, \Gamma_1 = (\alpha_h + \mu_h)E_h, \Gamma_2 = (\eta + \kappa + \mu_h)I_{ha}, \Gamma_3 = \mu_h I_{hc}, \Gamma_4 = (\delta + \omega_1(1-\delta) + \mu_h)T_h, \Gamma_5 = (\rho + \mu_h)W_h, \Gamma_6 = (\omega_2 + \eta_1 + \mu_h)R_1, \Gamma_7 = (\omega_3 + \eta_2 + \mu_h)R_2, \Gamma_8 = (\eta_3 + \mu_h)R_3, \Gamma_9 = (\alpha_m + \mu_h)E_m, \Gamma_{10} = \mu_m I_m$

Specifically if, $Y_1(0) > 0$ then $Y_1(t) \geq 0 \ \forall t \geq 0$. Applying the variation of the constant formula, we have

$$0 \leq Y_1(t) = e^{A_1 t} Y_1(0) - \int_0^t e^{A_1(t-r)} \hat{G}(X_1(r), Y_1(r))\, dr \leq e^{A_1 t} Y_1(0),$$

since A_1 is M-matrix ,$\mathcal{R}_0 < 1$ then A_1 had a negative dominant eigenvalues,

$$\lim_{t \to \infty} \| e^{A_1(t)} \| = 0$$

$$\lim_{t \to \infty} Y_1(t) = 0$$

□

These prove that model 2.5 is globally stable.

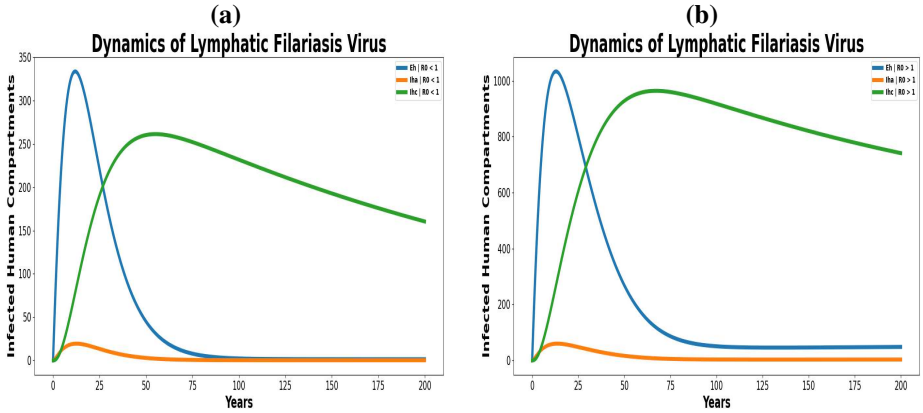


Figure 3: Global stability of lymphatic filariasis at disease-free equilibrium when **(a) and (b)** $\mathcal{R}_0 = 1$**. All simulations were conducted using the baseline parameter values provided in Table ??**

The global stability of the disease-free equilibrium (DFE), E_0, of the lymphatic filariasis model is validated under two scenarios. First, when $\mathcal{R}_0$ is less than unity ($\mathcal{R}_0 < 1$), using all parameter values as indicated in Table 3, except for $\beta = 1.322$ and $\mathcal{R}_0 = 0.05$. Secondly, as shown in 4(b), the global stability of the DFE is demonstrated when $\mathcal{R}_0 = 1$ is obtained with $\beta = 26.445$ and $\mathcal{R}_0 = 1.0$, while all other parameters remain as listed in Table 3.

3.4 Endemic Equilibrium

The endemic equilibrium state of model 2.5 is determined if disease persists in a population at a constant level over time, without dying out or leading to an outbreak however, the endemic equilibrium is given as:

$$T^* = (S_h^*, E_h^*, I_{ha}^*, I_{hc}^*, T_h^*, W_h^*, R_1^*, R_2^*, R_3^*, S_m^*, E_m^*, I_m^*)$$

$$\begin{cases} 0 = \Lambda_h + \rho W_h^* - \dfrac{\beta\vartheta_h I_m^* S_h^*}{N_h} - \mu_h S_h^* \\ 0 = \dfrac{\beta\vartheta_h I_m^* S_h^*}{N_h} - (\alpha_h + \mu_h)E_h^* \\ 0 = \alpha_h E_h^* - \eta I_{ha}^* - (\kappa + \mu_h)I_{ha}^* \\ 0 = \kappa I_{ha}^* - \mu_h I_{hc}^* \\ 0 = \eta I_{ha}^* - (\eta + \omega_1(1-\delta) + \mu_h)T_h^* \\ 0 = \delta T_h^* + \eta_1 R_1^* + \eta_2 R_2^* + \eta_3 R_3^* - (\rho + \mu_h)W_h^* \\ 0 = \omega_1(1-\delta)T_h^* - (\omega_2 + \eta_1 + \mu_h)R_1^* \\ 0 = \omega_2 R_1^* - (\omega_3 + \eta_2 + \mu_h)R_2^* \\ 0 = \omega_3 R_2^* - (\eta_3 + \mu_h)R_3^* \\ 0 = \Lambda_m - \dfrac{\beta\vartheta_m(I_{ha}^* + \delta I_{hc}^*)S_m^*}{N_h^*} - \mu_m S_m^* \\ 0 = \dfrac{\beta\vartheta_m(I_{ha}^* + \delta I_{hc}^*)S_m^*}{N_h} - (\alpha_m + \mu_m)E_m^* \\ 0 = \alpha_m E_m^* - \mu_m I_m^* \end{cases} \tag{3.15}$$

Solving the system 3.15 when it is in a general steady state, the following results are obtained:

$$S_h^* = \frac{\Lambda_h(\alpha_h+\mu_h)(\eta+\kappa+\mu_h)(\eta+\omega1(1-\delta)+\mu_h)(\rho+\mu_h)(\omega2+\eta1+\mu_h)(\omega3+\eta2+\mu_h)(\eta3+\mu_h)}{\alpha_h\eta\eta_3\lambda_h^*\omega_2\omega_3\rho\xi_{11} + \alpha_h\eta\eta_2\lambda_h^*\omega_2\rho\xi_{11}\xi_8 + \alpha_h\eta\eta_1\lambda_h^*\rho\xi_{11}\xi_7\xi_8 + \alpha_h\delta\eta\lambda_h^*\rho\xi_6\xi_7\xi_8 - (\lambda_h+\mu_h)\prod}$$

$$E_h^* = \frac{\Lambda_h\lambda_h^*(\eta+\kappa+\mu_h)(\eta+\omega1(1-\delta)+\mu_h)(\rho+\mu_h)(\omega2+\eta1+\mu_h)(\omega3+\eta2+\mu_h)(\eta3+\mu_h)}{\alpha_h\eta\eta_3\lambda_h^*\omega_2\omega_3\rho\xi_{11} + \alpha_h\eta\eta_2\lambda_h^*\omega_2\rho\xi_{11}\xi_8 + \alpha_h\eta\eta_1\lambda_h^*\rho\xi_{11}\xi_7\xi_8 + \alpha_h\delta\eta\lambda_h^*\rho\xi_6\xi_7\xi_8 - (\lambda_h+\mu_h)\prod}$$

$$I_{ha}^* = \frac{\Lambda_h\alpha_h\lambda_h^*(\eta+\omega1(1-\delta)+\mu_h)(\rho+\mu_h)(\omega2+\eta1+\mu_h)(\omega3+\eta2+\mu_h)(\eta3+\mu_h)}{\alpha_h\eta\eta_3\lambda_h^*\omega_2\omega_3\rho\xi_{11} + \alpha_h\eta\eta_2\lambda_h^*\omega_2\rho\xi_{11}\xi_8 + \alpha_h\eta\eta_1\lambda_h^*\rho\xi_{11}\xi_7\xi_8 + \alpha_h\delta\eta\lambda_h^*\rho\xi_6\xi_7\xi_8 - (\lambda_h+\mu_h)\prod}$$

$$I_{hc}^* = \frac{\Lambda_h\alpha_h\kappa\lambda_h^*(\eta+\omega1(1-\delta)+\mu_h)(\rho+\mu_h)(\omega2+\eta1+\mu_h)(\omega3+\eta2+\mu_h)(\eta3+\mu_h)}{\left(\alpha_h\eta\eta_3\lambda_h^*\omega_2\omega_3\rho\xi_{11} + \alpha_h\eta\eta_2\lambda_h^*\omega_2\rho\xi_{11}\xi_8 + \alpha_h\eta\eta_1\lambda_h^*\rho\xi_{11}\xi_7\xi_8 + \alpha_h\delta\eta\lambda_h^*\rho\xi_6\xi_7\xi_8 - (\lambda_h+\mu_h)\prod\right)\mu_h}$$

$$T_h^* = \frac{\Lambda_h \alpha_h \eta \lambda_h^* (\rho + \mu_h)(\omega 2 + \eta 1 + \mu_h)(\omega 3 + \eta 2 + \mu_h)(\eta 3 + \mu_h)}{\alpha_h \eta\eta_3 \lambda_h^* \omega_2 \omega_3 \rho \xi_{11} + \alpha_h \eta\eta_2 \lambda_h^* \omega_2 \rho \xi_{11} \xi_8 + \alpha_h \eta\eta_1 \lambda_h^* \rho \xi_{11} \xi_7 \xi_8 + \alpha_h \delta \eta \lambda_h^* \rho \xi_6 \xi_7 \xi_8 - (\lambda_h + \mu_h) \prod}$$

$$W_h^* = \frac{(\eta_3 \omega_2 \omega_3 \xi_{11} + \eta_2 \omega_2 \xi_{11} \xi_8 + \eta_1 \xi_{11} \xi_7 \xi_8 + \delta \xi_6 \xi_7 \xi_8) \Lambda_h \alpha_h \eta \lambda_h^*}{\alpha_h \eta\eta_3 \lambda_h^* \omega_2 \omega_3 \rho \xi_{11} + \alpha_h \eta\eta_2 \lambda_h^* \omega_2 \rho \xi_{11} \xi_8 + \alpha_h \eta\eta_1 \lambda_h^* \rho \xi_{11} \xi_7 \xi_8 + \alpha_h \delta \eta \lambda_h^* \rho \xi_6 \xi_7 \xi_8 - (\lambda_h + \mu_h) \prod}$$

$$R_1^* = \frac{\Lambda_h \alpha_h \eta \lambda_h^* \omega 1 (1 - \delta)(\rho + \mu_h)(\omega 3 + \eta 2 + \mu_h)(\eta 3 + \mu_h)}{\alpha_h \eta\eta_3 \lambda_h^* \omega_2 \omega_3 \rho \xi_{11} + \alpha_h \eta\eta_2 \lambda_h^* \omega_2 \rho \xi_{11} \xi_8 + \alpha_h \eta\eta_1 \lambda_h^* \rho \xi_{11} \xi_7 \xi_8 + \alpha_h \delta \eta \lambda_h^* \rho \xi_6 \xi_7 \xi_8 - (\lambda_h + \mu_h) \prod}$$

$$R_2^* = \frac{\Lambda_h \alpha_h \eta \lambda_h^* \omega_2 \omega 1 (1 - \delta)(\rho + \mu_h)(\eta 3 + \mu_h)}{\alpha_h \eta\eta_3 \lambda_h^* \omega_2 \omega_3 \rho \xi_{11} + \alpha_h \eta\eta_2 \lambda_h^* \omega_2 \rho \xi_{11} \xi_8 + \alpha_h \eta\eta_1 \lambda_h^* \rho \xi_{11} \xi_7 \xi_8 + \alpha_h \delta \eta \lambda_h^* \rho \xi_6 \xi_7 \xi_8 - (\lambda_h + \mu_h) \prod}$$

$$R_3^* = \frac{\Lambda_h \alpha_h \eta \lambda_h^* \omega_2 \omega_3 \omega 1 (1 - \delta)(\rho + \mu_h)}{\alpha_h \eta\eta_3 \lambda_h^* \omega_2 \omega_3 \rho \xi_{11} + \alpha_h \eta\eta_2 \lambda_h^* \omega_2 \rho \xi_{11} \xi_8 + \alpha_h \eta\eta_1 \lambda_h^* \rho \xi_{11} \xi_7 \xi_8 + \alpha_h \delta \eta \lambda_h^* \rho \xi_6 \xi_7 \xi_8 - (\lambda_h + \mu_h) \prod}$$

$$S_m^* = \frac{\Lambda_m}{\lambda_m^* + \mu_m}$$

$$E_m^* = \frac{\Lambda_m \lambda_m^*}{(\alpha_m + \mu_m)(\lambda_m^* + \mu_m)}$$

$$I_m^* = \frac{\Lambda_m \alpha_m \lambda_m^*}{(\alpha_m + \mu_m)(\lambda_m^* + \mu_m)\mu_m},$$

where, $\xi_2 = (\alpha_h + \mu_h)$, $\xi_3 = (\eta + \kappa + \mu_h)$, $\xi_4 = (\eta + \omega 1(1 - \delta) + \mu_h)$, $\xi_5 = (\rho + \mu_h)$, $\xi_6 = (\omega 2 + \eta 1 + \mu_h)$, $\xi_7 = (\omega 3 + \eta 2 + \mu_h)$, $\xi_8 = (\eta 3 + \mu_h)$, $\xi_{11} = \omega 1(1 - \delta)$, and $\prod = \xi_2 \xi_3 \xi_4 \xi_5 \xi_6 \xi_7 \xi_8$.

Lemma 3.3. *A unique endemic equilibrium exists in the lymphatic filariasis model 2.5 whenever $\mathcal{R}_0 > 1$; otherwise, no endemic equilibrium is present.*

Proof. To establish the global stability of the endemic equilibrium, we construct a logarithmic Lyapunov function following the approach proposed by [12] given as:

$$V = \sum_{j=1}^{12} \left(\omega_j - \omega_j^* - \omega_j^* \ln \left(\frac{\omega_j}{\omega_j^*} \right) \right),$$

where ω_j represents the j-th feasible state variable, and ω_j^* denotes its corresponding endemic equilibrium value principle.

We obtained:

$$\begin{aligned} V = {} & (S_h - S_h^*) - S_h^* \ln \left(\frac{S_h^*}{S_h} \right) + h_1 (S_m - S_m^*) - S_m^* \ln \left(\frac{S_m^*}{S_m} \right) + h_2 (E_h - E_h^*) - E_h^* \ln \left(\frac{E_h^*}{E_h} \right) + h_3 (I_{ha} - I_{ha}^*) - I_{ha}^* \ln \left(\frac{I_{ha}^*}{I_{ha}} \right) \\ & + h_4 (I_{hc} - I_{hc}^*) - I_{hc}^* \ln \left(\frac{I_{hc}^*}{I_{hc}} \right) + h_5 (T_h - T_h^*) - T_h^* \ln \left(\frac{T_h^*}{T_h} \right) + h_6 (W_h - W_h^*) - W_h^* \ln \left(\frac{W_h^*}{W_h} \right) + h_7 (R_1 - R_1^*) - R_1^* \ln \left(\frac{R_1^*}{R_1} \right) \\ & + h_8 (R_2 - R_2^*) - R_2^* \ln \left(\frac{R_2^*}{R_2} \right) + h_9 (R_3 - R_3^*) - R_3^* \ln \left(\frac{R_3^*}{R_3} \right) + h_{10} (E_m - E_m^*) - E_m^* \ln \left(\frac{E_m^*}{E_m} \right) + h_{11} (I_m - I_m^*) - I_m^* \ln \left(\frac{I_m^*}{I_m} \right). \end{aligned} \tag{3.16}$$

We calculate the time derivative of $V(X)$. For a logarithmic Lyapunov function, this can be expressed as:

$$
\begin{aligned}
\dot{V} = &\left(1-\frac{S_h^*}{S_h}\right)\left[\Lambda_h+\rho W_h-(\lambda_h^*+\mu_h)S_h\right]+\left(1-\frac{E_h^*}{E_h}\right)\left[\lambda_h^* S_h-(\alpha_h+\mu_h)E_h\right]\\
&+\left(1-\frac{I_{ha}^*}{I_{ha}}\right)\left[\alpha_h E_h-(\eta+\kappa+\mu_h)I_{ha}\right]+\left(1-\frac{I_{hc}^*}{I_{hc}}\right)\left[\kappa I_{ha}-\mu_h I_{hc}\right]\\
&+\left(1-\frac{T_h^*}{T_h}\right)\left[\eta I_{ha}-(\delta+\omega_1(1-\delta)+\mu_h)T_h\right]+\left(1-\frac{W_h^*}{W_h}\right)\left[\delta T_h+\eta_1 R_1+\eta_2 R_2+\eta_3 R_3-(\rho+\mu_h)W_h\right]\\
&+\left(1-\frac{R_1^*}{R_1}\right)\left[\omega_1(1-\delta)T_h-(\omega_2+\eta_1+\mu_h)R_1\right]+\left(1-\frac{R_2^*}{R_2}\right)\left[\omega_2 R_1-(\omega_3+\eta_2+\mu_h)R_2\right]\\
&+\left(1-\frac{R_3^*}{R_3}\right)\left[\omega_3 R_2-(\eta_3+\mu_h)R_3\right]+\left(1-\frac{S_m^*}{S_m}\right)\left[\Lambda_m-(\lambda_m^*+\mu_m)S_m\right]\\
&+\left(1-\frac{E_m^*}{E_m}\right)\left[\lambda_m^* S_m-(\alpha_m+\mu_m)E_m\right]+\left(1-\frac{I_m^*}{I_m}\right)\left[\alpha_m E_m-\mu_m I_m\right].
\end{aligned}
\tag{3.17}
$$

By expanding and simplifying the expression we have,

$$
\begin{aligned}
\dot{V} = &\Lambda_h+\rho W_h-(\lambda_h^*+\mu_h)S_h-\frac{S_h^*}{S_h}(\Lambda_h+\rho W_h)+S_h^*(\lambda_h^*+\mu_h)+\lambda_h^* S_h-(\alpha_h+\mu_h)E_h-\frac{E_h^*}{E_h}\lambda_h^* S_h+E_h^*(\alpha_h+\mu_h)\\
&+\alpha_h E_h-(\eta+\kappa+\mu_h)I_{ha}-\frac{I_{ha}^*}{I_{ha}}\alpha_h E_h+I_{ha}^*(\eta+\kappa+\mu_h)+\kappa I_{ha}-\mu_h I_{hc}-\frac{I_{hc}^*}{I_{hc}}\kappa I_{ha}+I_{hc}^*\mu_h\\
&+\eta I_{ha}-(\delta+\omega_1(1-\delta)+\mu_h)T_h-\frac{T_h^*}{T_h}\eta I_{ha}+T_h^*(\delta+\omega_1(1-\delta)+\mu_h)\\
&+\delta T_h+\eta_1 R_1+\eta_2 R_2+\eta_3 R_3-(\rho+\mu_h)W_h-\frac{W_h^*}{W_h}(\delta T_h+\eta_1 R_1+\eta_2 R_2+\eta_3 R_3)+W_h^*(\rho+\mu_h)\\
&+\omega_1(1-\delta)T_h-(\omega_2+\eta_1+\mu_h)R_1-\frac{R_1^*}{R_1}\omega_1(1-\delta)T_h+R_1^*(\omega_2+\eta_1+\mu_h)\\
&+\omega_2 R_1-(\omega_3+\eta_2+\mu_h)R_2-\frac{R_2^*}{R_2}\omega_2 R_1+R_2^*(\omega_3+\eta_2+\mu_h)+\omega_3 R_2-(\eta_3+\mu_h)R_3-\frac{R_3^*}{R_3}\omega_3 R_2+R_3^*(\eta_3+\mu_h)\\
&+\Lambda_m-(\lambda_m^*+\mu_m)S_m-\frac{S_m^*}{S_m}\Lambda_m+S_m^*(\lambda_m^*+\mu_m)+\lambda_m^* S_m-(\alpha_m+\mu_m)E_m\\
&-\frac{E_m^*}{E_m}\lambda_m^* S_m+E_m^*(\alpha_m+\mu_m)+\alpha_m E_m-\mu_m I_m-\frac{I_m^*}{I_m}\alpha_m E_m+I_m^*\mu_m.
\end{aligned}
$$

Let

$$\dot{V} = V_1 - V_2,$$

where V_1 and V_2 are given by

$$
\begin{aligned}
V_1 = &S_h^*(\lambda_h^*+\mu_h)+E_h^*(\alpha_h+\mu_h)+I_{ha}^*(\eta+\kappa+\mu_h)+I_{hc}^*\mu_h \quad +T_h^*(\delta+\omega_1(1-\delta)+\mu_h)+W_h^*(\rho+\mu_h)\\
&+R_1^*(\omega_2+\eta_1+\mu_h) \quad +R_2^*(\omega_3+\eta_2+\mu_h)+R_3^*(\eta_3+\mu_h)+S_m^*(\lambda_m^*+\mu_m)\\
&+E_m^*(\alpha_m+\mu_m)+I_m^*\mu_m+\Lambda_h+\rho W_h+\lambda_h^* S_h+\alpha_h E_h \quad +\kappa I_{ha}+\eta I_{ha}+\delta T_h+\eta_1 R_1+\eta_2 R_2+\eta_3 R_3\\
&+\omega_1(1-\delta)T_h+\omega_2 R_1+\omega_3 R_2+\Lambda_m+\lambda_m^* S_m+\alpha_m E_m
\end{aligned}
\tag{3.18}
$$

and

$$
\begin{aligned}
V_2 = &(\lambda_h^*+\mu_h)S_h+\frac{S_h^*}{S_h}(\Lambda_h+\rho W_h)+(\alpha_h+\mu_h)E_h \quad +\frac{E_h^*}{E_h}\lambda_h^* S_h+(\eta+\kappa+\mu_h)I_{ha}+\frac{I_{ha}^*}{I_{ha}}\alpha_h E_h\\
&+\mu_h I_{hc}+\frac{I_{hc}^*}{I_{hc}}\kappa I_{ha}+(\delta+\omega_1(1-\delta)+\mu_h)T_h+\frac{T_h^*}{T_h}\eta I_{ha} \quad +(\rho+\mu_h)W_h+\frac{W_h^*}{W_h}(\delta T_h+\eta_1 R_1+\eta_2 R_2+\eta_3 R_3)\\
&+(\omega_2+\eta_1+\mu_h)R_1+\frac{R_1^*}{R_1}\omega_1(1-\delta)T_h+(\omega_3+\eta_2+\mu_h)R_2 \quad +\frac{R_2^*}{R_2}\omega_2 R_1+(\eta_3+\mu_h)R_3+\frac{R_3^*}{R_3}\omega_3 R_2\\
&+(\lambda_m^*+\mu_m)S_m+\frac{S_m^*}{S_m}\Lambda_m+(\alpha_m+\mu_m)E_m+\frac{E_m^*}{E_m}\lambda_m^* S_m+\mu_m I_m+\frac{I_m^*}{I_m}\alpha_m E_m.
\end{aligned}
\tag{3.19}
$$

If $\dot{V}_1 < \dot{V}_2$, then $\dot{V} \leq 0$. Based on LaSalle's invariant principle, the endemic equilibrium T^* achieves global asymptotic stable, where $\dot{V} = 0$ hold if and only if $Q = T^*$. where

$Q = (S_h, E_h, I_{ha}, I_{hc}, T_h, W_h, R_1, R_2, R_3, S_m, E_m, I_m)$

$T^* = (S_h^*, E_h^*, I_{ha}^*, I_{hc}^*, T_h^*, W_h^*, R_1^*, R_2^*, R_3^*, S_m^*, E_m^*, I_m^*)$

Hence, the largest compact invariant set is contained within.

$$\left\{(S_h, E_h, I_{ha}, I_{hc}, T_h, W_h, R_1, R_2, R_3, S_m, E_m, I_m) \in \mathbb{R}_+^{12} : \dot{V} = 0\right\} \tag{3.20}$$

We deduce that T^* is globally stable in $\mathbb{R}_+^{12}$, provided $\mathcal{R}_0 > 1$. □

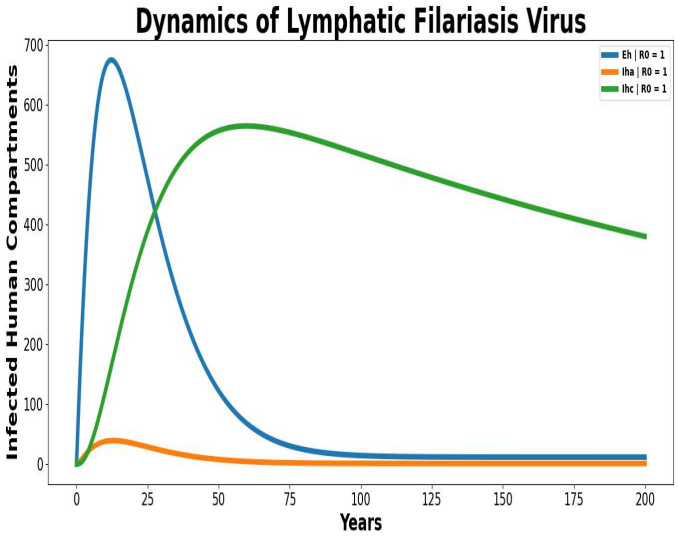


Figure 4: Global stability of infected humans at Equilibrium when $\mathcal{R}_0 > 1$. All simulations were conducted using the baseline parameter values provided in Table 3.

The global stability of the infected humans at equilibrium when ($\mathcal{R}_0 > 1$) of the lymphatic filariasis model is validated when $\mathcal{R}_0$ is greater than unity ($\mathcal{R}_0 > 1$), using all parameter values as indicated in Table 3, except for $\beta = 39.666803$ and $\mathcal{R}_0 = 1.5$. while all other parameters remain as listed in Table 3.

4 Parameter Estimation

To quantify the dynamics of lymphatic filariasis (LF) transmission in Ghana, we calibrated the proposed model using empirical data extracted from the national monitoring reports published in [2]. The dataset consists of yearly aggregated counts of individuals who tested positive for microfilariae (mf) from 2010 to 2014 across selected endemic districts. These data were collected as part of Ghana's post-MDA (Mass Drug Administration) surveillance efforts during the country's transition toward elimination.

4.1 Fitting Strategy

The model was fitted to the observed cumulative mf-positive cases using a nonlinear least squares method implemented via MATLAB's `lsqcurvefit` optimizer. A Savitzky-Golay filter was first applied to the differenced infection counts to smooth local fluctuations while preserving the overall trend. The fitting objective was to minimize the sum of squared residuals between observed values $y_{\text{obs}}(t)$ and model-predicted values $y_{\text{model}}(t; \boldsymbol{\theta})$, given by:

$$\min_{\boldsymbol{\theta}} \sum_{i=1}^{n} \left[y_{\text{obs}}(t_i) - y_{\text{model}}(t_i; \boldsymbol{\theta})\right]^2 .$$

This optimization yielded parameter values $\boldsymbol{\theta}$ that best describe the observed progression of LF in the target population.

Next, we present the estimated parameters and initial conditions. The estimation focused on four key biological parameters—progression rate to chronic infection (κ), worm recovery rate (ρ), first-stage recovery rate (ω_1), and transmission/contact rate (β)—as well as three initial conditions: susceptible population (S_{h0}), acute infections (I_{ha0}), and chronic infections (I_{hc0}). The fitted values are provided in Table 3.

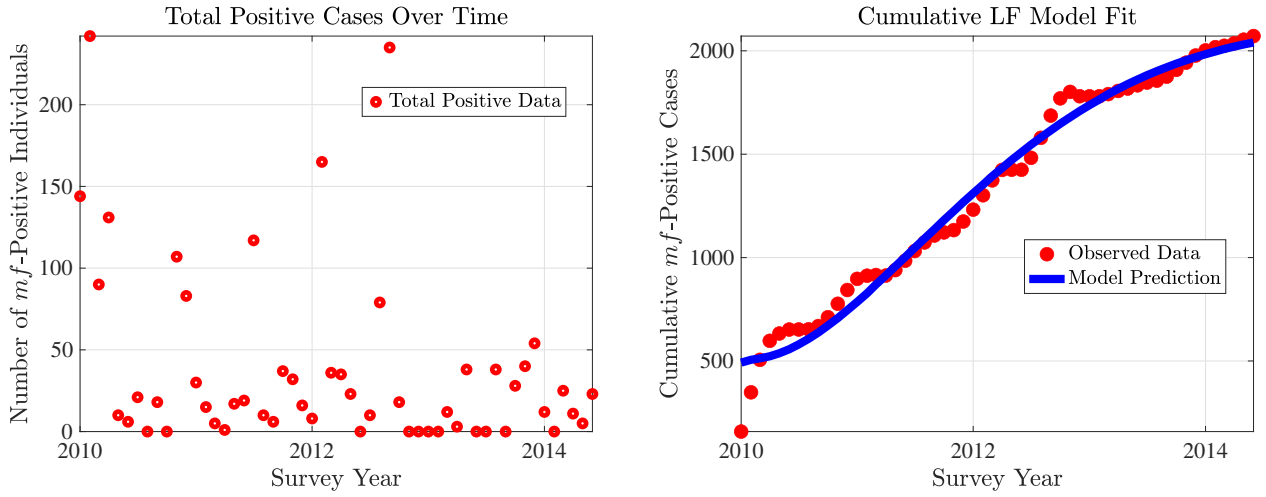


Figure 5: **(a)** Observed total number of individuals testing positive for microfilariae (mf) per survey year across Ghana's endemic districts. The data, drawn from [2], reflects year-to-year fluctuations during the post-MDA surveillance phase. **(b)** Model fit to the cumulative mf-positive cases. Red circles represent observed data, while the blue curve denotes the model prediction. The fitted model captures the upward trajectory of cumulative infections over time with high accuracy ($R^2 = 0.98$), supporting its utility for evaluating LF elimination progress.

In addition, to reduce model complexity and improve identifiability, several parameters were fixed based on estimates from the literature and biological assumptions. The fixed parameters include demographic rates, transition probabilities, and transmission-related constants. Table **??** summarizes their values.

Table 3: Estimated parameters and initial conditions for the LF model fit to Ghana data.

Parameter	**Description**	**Estimated Value**
κ	Progression to chronic infection	0.5368
ρ	Worm recovery rate	0.0101
ω_1	First-stage recovery rate	1.1211e-05
β	Transmission/contact rate	43.8166
S_{h0}	Initial susceptible population	2,000,000
I_{ha0}	Initial acute mf-positive individuals	50
I_{hc0}	Initial chronic mf-positive individuals	492

The total initial human population was assumed to be $N_h = 1 \times 10^6$. Initial conditions for human compartments were derived as proportions of N_h: exposed individuals $E_h(0) = 10^{-9}N_h$, treated individuals $T_h(0) = 0.0002N_h$, chronic stage individuals $W_h(0) = 0.00001N_h$, and recovered compartments $R_1(0) = R_2(0) = R_3(0) = 0$. The remaining population was assigned to the susceptible class $S_h(0)$ such that mass balance was preserved:

$$S_h(0) = N_h - (E_h(0) + I_{ha}(0) + I_{hc}(0) + T_h(0) + W_h(0) + R_1(0) + R_2(0) + R_3(0)),$$

where $I_{ha}(0)$ and $I_{hc}(0)$ were estimated from data fitting. The initial mosquito population was set to 1×10^4, distributed as follows: susceptible $S_m(0) = 0.9 \times 10^4$, exposed $E_m(0) = 0.005 \times 10^4$, and infectious $I_m(0) = 0.005 \times 10^4$.

4.2 Confidence Intervals and Goodness-of-Fit

Using the Jacobian returned by the optimizer, we computed 95% confidence intervals for each parameter. The model demonstrated a strong agreement with the observed data, yielding a coefficient of determination of $R^2 = 0.9797$. This indicates that the model explains nearly 98% of the variability in the cumulative mf-positive case counts, underscoring its ability to reproduce LF dynamics during Ghana's elimination phase.

4.3 Residual Diagnostics and Model Adequacy

While the R^2 value of 0.98 (Figure 5) indicates that the model reproduces the general trend in the cumulative *mf*-positive data, a high value R^2 alone does not guarantee that the model fully captures the underlying transmission dynamics. To assess the adequacy of the fitted model, we conducted a detailed residual analysis (Figure 6) using standardized residuals, distributional checks, autocorrelation analysis, and normal Q–Q plots.

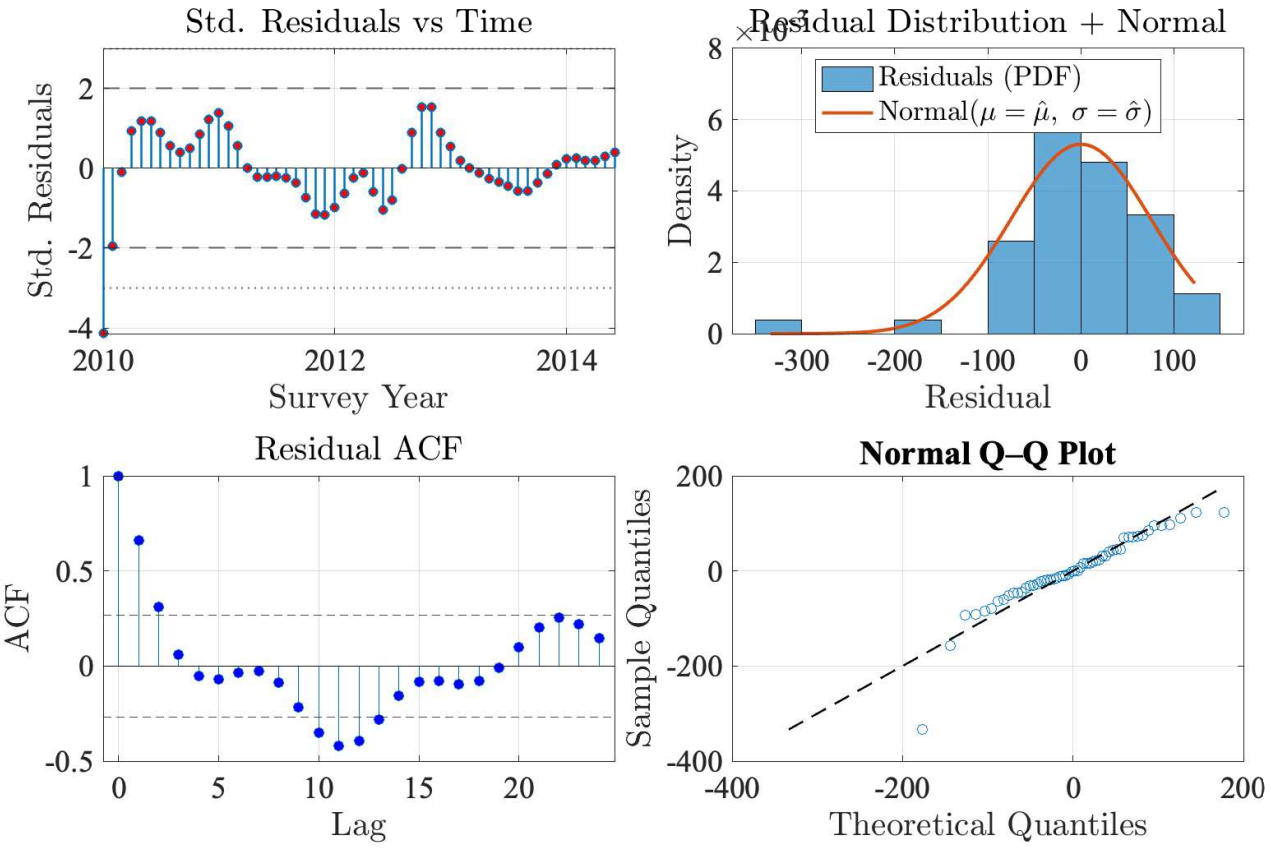


Figure 6: Residual diagnostics for the calibrated LF model: (a) standardized residuals vs. time with $\pm 2\sigma$ and $\pm 3\sigma$ reference lines; (b) histogram of residuals with fitted normal density; (c) residual autocorrelation function (ACF) with 95% confidence bounds; (d) normal Q–Q plot.

We present the standardized residuals vs. time in Figure 6(a). Most deviations fell within the $\pm 2\sigma$ bounds, suggesting no extreme outliers. However, distinct temporal clusters of positive and negative residuals were observed, notably in mid-2010 to early 2011 (overestimation) and mid-2011 to early 2012 (underestimation). Such clustering suggests that unmodeled time-dependent processes such as seasonality, variations in intervention coverage, or localized outbreak effects may influence transmission dynamics. In Figure 6(b), we present the residual distribution analysis. The histogram exhibited a left-skew relative to the fitted normal density, with heavier negative tails. This indicates that the model occasionally underestimates the observed prevalence by a substantial margin, particularly at the beginning of the time series. The Autocorrelation function (ACF) as seen in Figure 6(c) displayed statistically significant short-lag correlations, implying that residuals are not fully independent and may contain unmodeled temporal structure. This is consistent with the possibility of serial correlation arising from environmental or programmatic factors operating at annual or sub-annual timescales. Finally, the Normal Q–Q plot is seen in Figure 6(d) where deviations from the 45° line were most pronounced in the lower tail, where large negative residuals occurred more often than expected under Gaussian assumptions. This suggests potential structural mismatches during specific years, possibly linked to un-accounted shocks in transmission.

5 Sensitivity Analysis

The impact of model parameters on the basic reproduction number ($\mathcal{R}_0$) of lymphatic filariasis was assessed using sensitivity analysis to identify parameters that most influence disease transmission. Parameters related to mosquitoes, transmission, treatment, infection progression, and immunity were analyzed using values from Table 3. Latin Hypercube Sampling (LHS)

was used, varying each parameter by ±20% around its baseline value over 5000 simulation runs. Partial Rank Correlation Coefficients (PRCCs) quantified the monotonic relationship between each parameter and $\mathcal{R}_0$, controlling for all others. Statistical significance was determined using a two-tailed test for correlation coefficients. The results are summarized in Figure 7. Mosquito-related parameters strongly influenced $\mathcal{R}_0$. The natural death rate of mosquitoes (μ_m) was negatively correlated (PRCC = -0.958, $p < 0.001$), while mosquito recruitment (Λ_m, PRCC = 0.789, $p < 0.001$), progression to infectious stage (α_m, PRCC = 0.568, $p < 0.001$), and human-to-mosquito transmission probability (ϑ_m, PRCC = 0.789, $p < 0.001$) were positively correlated. Transmission parameters, including mosquito biting rate (β, PRCC = 0.934, $p < 0.001$) and mosquito-to-human transmission probability (ϑ_h, PRCC = 0.792, $p < 0.001$), also strongly affected $\mathcal{R}_0$. Treatment rate of acutely infected humans (η, PRCC = -0.623, $p < 0.001$) reduced $\mathcal{R}_0$, while partial immunity acquisition (δ, PRCC = 0.782, $p < 0.001$) and progression from acute to chronic infection (κ, PRCC = 0.615, $p < 0.001$) increased it. Moderately influential parameters included human death rate (μ_h, PRCC = -0.050) and progression from exposed to acutely infected humans (α_h, PRCC = 0.042). Other parameters, such as immunity development and loss rates, had negligible effects. These results suggest that control strategies should prioritize mosquito mortality, recruitment, biting rate, transmission probabilities, and treatment effectiveness, while less influential parameters can be deprioritized. The use of 5000 LHS samples ensures robust and reliable ranking of parameter importance for guiding interventions.

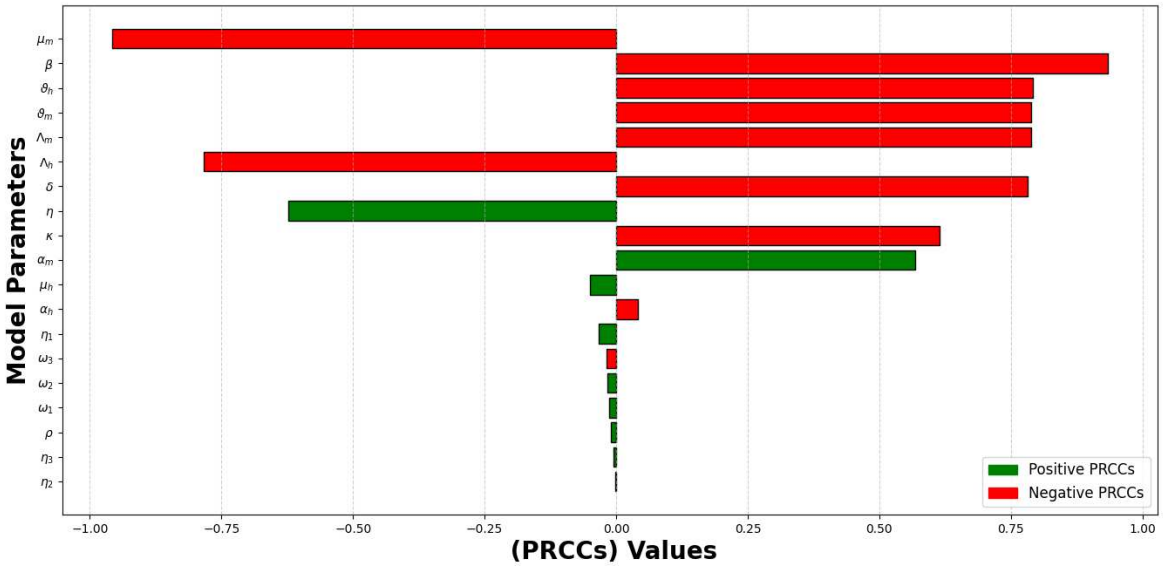


Figure 7: Tornado plot of Partial Rank Correlation Coefficients (PRCCs) values for some significant parameters on $\mathcal{R}_0$.

6 Numerical Simulations

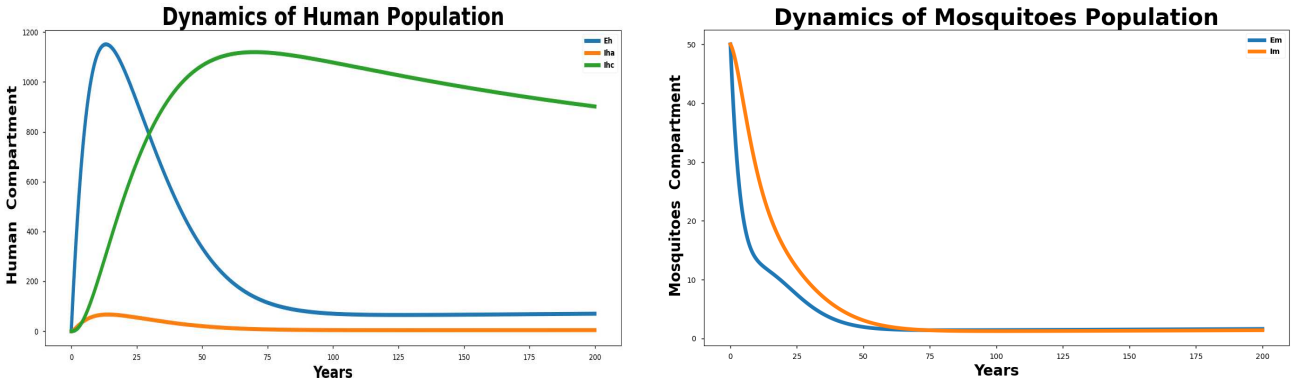
The simulations of the model 2.5 are carried out using python. The parameter values utilized in the model simulations are presented in Table 3 to exemplify some analytical findings. The total initial human population was assumed to be $N_h = 1\times10^6$. Initial conditions for human compartments were derived as proportions of N_h: exposed individuals $E_h(0) = 10^{-9}N_h$, treated individuals $T_h(0) = 0.0002N_h$, chronic stage individuals $W_h(0) = 0.00001N_h$, and recovered compartments $R_1(0) = R_2(0) = R_3(0) = 0$. The remaining population was assigned to the susceptible class $S_h(0)$ such that mass balance was preserved:

$$S_h(0) = N_h - (E_h(0) + I_{ha}(0) + I_{hc}(0) + T_h(0) + W_h(0) + R_1(0) + R_2(0) + R_3(0)),$$

where $I_{ha}(0)$ and $I_{hc}(0)$ were estimated from data fitting. The initial mosquito population was set to 1×10^4, distributed as follows: susceptible $S_m(0) = 0.9 \times 10^4$, exposed $E_m(0) = 0.005 \times 10^4$, and infectious $I_m(0) = 0.005 \times 10^4$.

Figure 8(a) presents a graphical representation of the disease dynamics within the human population following the introduction of the pathogen without intervention. It is observed that the exposed population undergoes a significant and rapid increase, driven by vector-to-human transmission, reaching a peak of approximately 1,200 individuals around day 15. Subsequently, this population declines and stabilizes at a persistent endemic level of about 70 individuals. While acute infections are transient, the chronic infection compartment shows a gradual accumulation, peaking at over 1,100 individuals near day 75. This chronically infected group diminishes slowly, establishing itself as the primary long-term reservoir for sustained transmission. The epidemic progresses through an initial outbreak phase (Days 0–25), a transition phase (Days 25–100), and culminates in an endemic equilibrium where chronic cases perpetuate new exposures. The critical role of the vector population is illustrated in Figure 8(b). Although the initial number of infected mosquitoes decreases due to natural mortality,

the population does not vanish. Instead, a low-level endemic mosquito population is maintained through transmission from chronically infected humans, creating a stable cycle that links the two populations.



(a) (b)

Figure 8: Simulation of disease dynamics without public health interventions. (a) Human populations. (b) Vector population.

The influence of the treatment rate (η) on the dynamics of Lymphatic Filariasis is depicted in Figure 9. The simulations show a clear inverse relationship between the rate of treatment and the magnitude of the disease outbreak. A lower treatment rate ($\eta = 0.10$) corresponds to a higher basic reproduction number, $\mathcal{R}_0 = 2.48$, and results in a more severe infection peak, reaching nearly 160 acute cases. As the treatment rate is increased, the infection curves are observed to flatten considerably, an indication that fewer individuals are acutely infected. This suggests that effective treatment implementation is crucial for reducing the infectious period of acute cases, thereby limiting subsequent transmission.

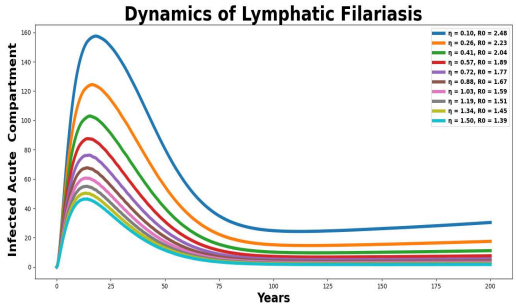


Figure 9: The impart of treatments on infected acute individuals For various treatment rate η values

Figure 10(a) illustrates the effect of treatment efficacy (δ) on the number of individuals who recover. The results indicate a direct and positive correlation; higher treatment efficacy leads to a greater number of recoveries. A high efficacy value ($\delta = 1.50$) results in the most favorable outcome, with the recovered population peaking at over 1,750. Conversely, a low efficacy ($\delta = 0.10$) signifies less effective treatment, leading to a substantially lower peak of around 1,100 recovered individuals. This demonstrates that poor treatment efficacy reduces positive patient outcomes. Furthermore, the impact of drug efficacy on the development of resistance is shown in Figure 10(b). It is noted that low drug efficacy is a primary driver of resistance, resulting in the highest peak of resistant infections. As treatment efficacy is enhanced, the emergence of resistance is significantly suppressed. This indicates that highly effective drugs are vital for preventing the spread of resistance, even when disease transmissibility is high.

The effect of varying the transmission rate (β) and the mosquito mortality rate (μ_m) on infection dynamics is presented in Figure 11. As shown in Figures 11(a), (b), and (c), a higher transmission rate (β) amplifies the outbreak's intensity and accelerates its progression. The exposed, acute, and chronic compartments all exhibit larger peaks that occur earlier in the simulation. This shows that increased transmission not only creates a more severe initial outbreak but also establishes a larger, sustained reservoir of chronic infections, which poses a long-term public health challenge. In Figure 11(d), it is observed that there is a strong inverse relationship between the mosquito natural death rate (μ_m) and the basic reproduction number, $\mathcal{R}_0$. A low mortality rate ($\mu_m = 0.10$) leads to the highest $\mathcal{R}_0$ (1.96) and a sustained endemic state. As mosquito mortality increases, $\mathcal{R}_0$ is reduced. When $\mathcal{R}_0$ falls below unity, the outbreak fails to persist, and the exposed population trends toward zero. This finding underscores that even modest increases in vector mortality can shift the disease dynamics from endemic persistence to eventual elimination.

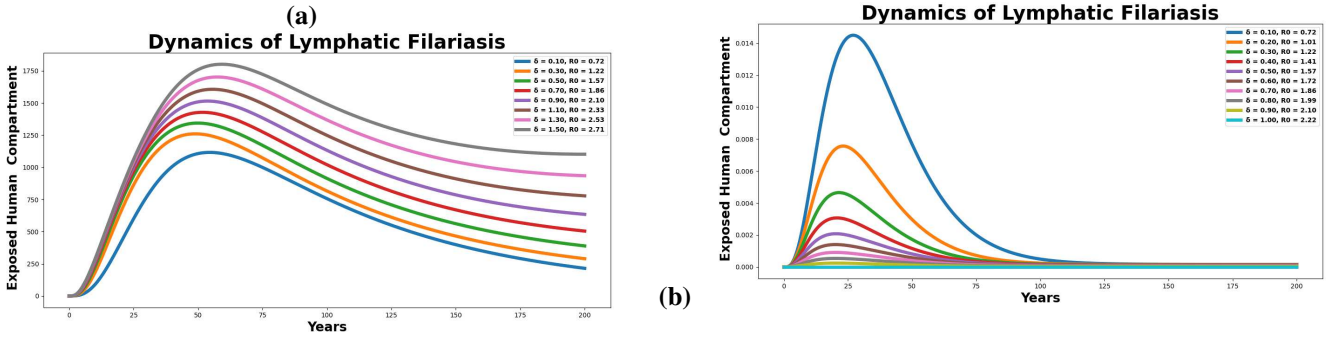


Figure 10: Impact of treatment efficacy on acutely infected individuals under different treatment rates δ.

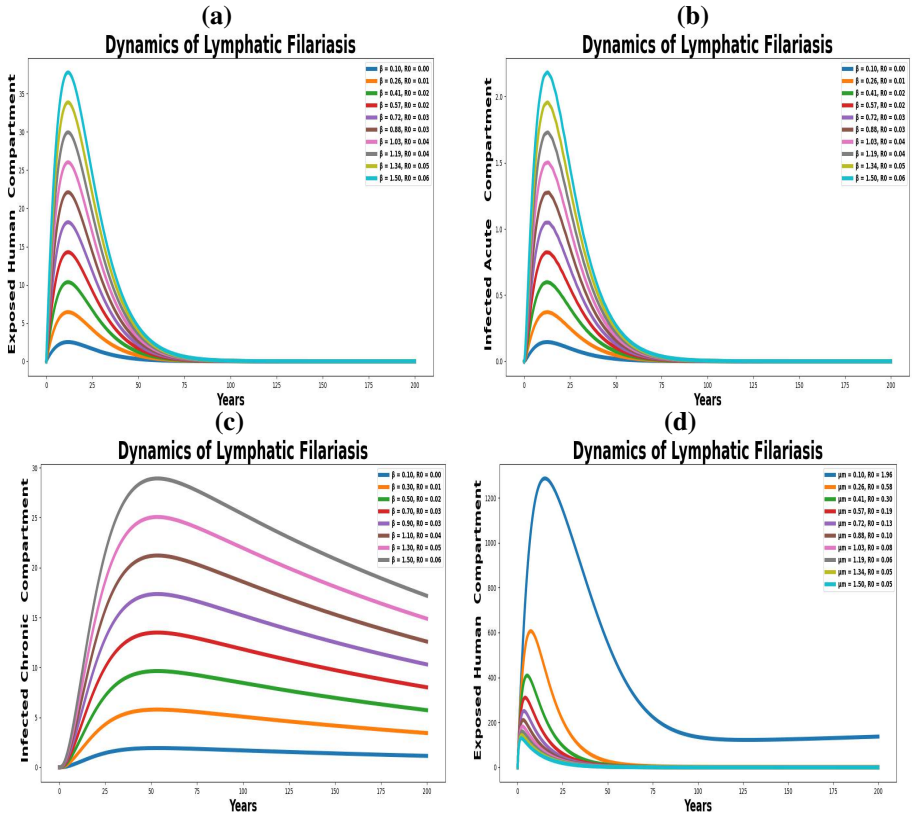


Figure 11: Dynamics of human infection compartments under varying transmission rates (β). on human populations

7 Conclusion and Recommendations

Lymphatic filariasis (LF) remains a substantial global public health challenge, causing chronic physical impairments and imposing significant socioeconomic costs. This study advanced the understanding of LF dynamics through a proposed SEIS mathematical model that uniquely integrates the latent phase, medical treatment, quarantine strategies, and the evolution of drug resistance, assessed using real-world post-MDA surveillance data from Ghana. The comprehensive approach through the lens of the basic reproduction number $\mathcal{R}_0$, revealed critical insights for effective disease control. Our findings strongly advocate for integrated intervention strategies. While medical treatment of acutely infected individuals was demonstrated to be more effective than quarantine in isolation, the most profound impact on reducing disease prevalence occurred when both medical treatment and quarantine of chronically infected patients were combined. The analysis also highlighted the paramount importance of vector control, with parameters such as mosquito natural death rate, recruitment, biting rate, and human-to-mosquito and mosquito-to-human transmission probabilities identified as the most influential factors on $\mathcal{R}_0$. Specifically, even modest increases in mosquito mortality were shown to be capable of shifting the disease dynamics from an endemic state towards eventual elimination. Furthermore, the study revealed the critical role of treatment efficacy, showing its direct correlation with patient recovery rates and its vital role in suppressing the emergence and dissemination of drug resistance, a growing challenge in antihelminthic treatments. While the model showed strong agreement with observed data ($R^2 = 0.98$), residual diagnostics suggested that future refinements could incorporate unmodeled temporal structures such as

seasonality or fluctuations in intervention coverage to further enhance predictive accuracy. In conclusion, effective control and elimination of lymphatic filariasis necessitate a multi-pronged approach that strategically combines high-coverage and highly efficacious medical treatments with robust vector control measures. Continuous monitoring for and mitigation of drug resistance are also essential components for the long-term success of LF elimination programs. These insights are crucial for informing public health policy, optimizing resource allocation, and guiding future research towards the global eradication of this debilitating disease.

Data Availability statement

Data sharing is not applicable to this article. The data used is open source and referenced in Section 4.

Conflict of Interest

The authors have no conflicts of interest to declare.

References

[1] DG Addiss. Global elimination of lymphatic filariasis: origins, progress and challenges. *Indian Journal of Urology*, 21 (1):12–17, 2005.

[2] Nana Kwadwo Biritwum, Kwadwo K Frempong, Suzanne Verver, Samuel Odoom, Bright Alomatu, Odame Asiedu, Periklis Kontoroupis, Abednego Yeboah, Edward Tei Hervie, Benjamin Marfo, et al. Progress towards lymphatic filariasis elimination in ghana from 2000-2016: Analysis of microfilaria prevalence data from 430 communities. *PLoS neglected tropical diseases*, 13(8):e0007115, 2019.

[3] G. Birkhoff and G. C. Rota. *Ordinary Differential Equations*. John Wiley & Sons, 4 edition, 1989.

[4] C. M. Bjerum, A. F. Ouattara, M. Aboulaye, O. Kouadio, V. K. Marius, B. J. Andersen, G. J. Weil, B. G. Koudou, and C. L. King. Efficacy and safety of a single dose of ivermectin, diethylcarbamazine, and albendazole for treatment of lymphatic filariasis in côte d'ivoire: An open-label randomized controlled trial. *Clinical Infectious Diseases*, 2020.

[5] Centers for Disease Control and Prevention. *Lymphatic filariasis*. U.S. Department of Health and Human Services, 2015.

[6] M. L. Eberhard, P. J. Lammie, and J. M. Roberts. Non-susceptibility to diethylcarbamazine in filarial worms. *Journal of Infectious Diseases*, 164, 1991.

[7] Timothy G Geary, Katherine Woo, James S McCarthy, Charles D Mackenzie, John Horton, Roger K Prichard, Nilanthi R de Silva, Piero L Olliaro, Janis K Lazdins-Helds, Dirk A Engels, et al. Unresolved issues in anthelmintic pharmacology for helminthiases of humans. *International journal for parasitology*, 40(1):1–13, 2010.

[8] Warwick N Grant. Genetic variation in parasitic nematodes and its implications. *International journal for parasitology*, 24(6):821–830, 1994.

[9] Patricia M Graves, Peter Wood, and Hervé C Bossin. Lymphatic filariasis in oceania. *Neglected Tropical Diseases-Oceania*, pages 101–142, 2016.

[10] T Déirdre Hollingsworth, Emily R Adams, Roy M Anderson, Katherine Atkins, Sarah Bartsch, María-Gloria Basáñez, Matthew Behrend, David J Blok, Lloyd AC Chapman, Luc Coffeng, et al. Quantitative analyses and modelling to support achievement of the 2020 goals for nine neglected tropical diseases. *Parasites & vectors*, 8(1):630, 2015.

[11] Jean Kamgang and Gérard Sallet. Computation of threshold conditions for epidemiological models and global stability of the disease-free equilibrium (dfe). *Mathematical Biosciences*, 213(1):1–12, 2008.

[12] A. Korobeinikov and G. C. Wake. Lyapunov functions and global stability for sir, sirs, and sis epidemiological models. *Applied Mathematics Letters*, 15, 2002.

[13] J. McCarter. Ivermectin resistance in Onchocerca volvulus: Toward a genetic basis. *PLoS Neglected Tropical Diseases*, 2007. doi: 10.1371/journal.pntd.0000076. URL https://doi.org/10.1371/journal.pntd.0000076.

[14] Wayne D Melrose. Lymphatic filariasis: new insights into an old disease. *International Journal for Parasitology*, 32(8): 947–960, 2002. ISSN 0020-7519.

[15] Peter M Mwamtobe, Simphiwe M Simelane, Shirley Abelman, and Jean M Tchuenche. Mathematical analysis of a lymphatic filariasis model with quarantine and treatment. *BMC Public Health*, 17(1):265, 2017.

[16] Eric A Ottesen, BO Duke, M Karam, and K Behbehani. Strategies and tools for the control/elimination of lymphatic filariasis. *Bulletin of the world Health Organization*, 75(6):491, 1997.

[17] Roger K. Prichard. Markers for benzimidazole resistance in human parasitic nematodes? *Parasitology*, 134(8):1087–1092, 2007. doi: 10.1017/S003118200700008X.

[18] L. C. Ranford-Cartwright and J. M. Mwangi. Analysis of malaria parasite phenotypes using experimental genetic crosses of *Plasmodium falciparum*. *International Journal for Parasitology*, 2012. doi: 10.1016/j.ijpara.2012.03.004. URL https://doi.org/10.1016/j.ijpara.2012.03.004.

[19] A. E. Schwab, D. A. Boakye, D. Kyelem, and R. K. Prichard. Detection of benzimidazole resistance-associated mutations in the filarial nematode *Wuchereria bancrofti* and evidence for selection by albendazole and ivermectin combination treatment. *American Journal of Tropical Medicine and Hygiene*, 73(2):234–238, August 2005. doi: 10.4269/ajtmh.2005.73.234.

[20] Wilma A Stolk, Sake J De Vlas, and J Dik F Habbema. Advances and challenges in predicting the impact of lymphatic filariasis elimination programmes by mathematical modelling. *Filaria Journal*, 5(1):5, 2006.

[21] Christopher M Stone, Steve W Lindsay, and Nakul Chitnis. How effective is integrated vector management against malaria and lymphatic filariasis where the diseases are transmitted by the same vector? *PLoS neglected tropical diseases*, 8(12):e3393, 2014.

[22] Henk Van den Berg, Louise A Kelly-Hope, and Steve W Lindsay. Malaria and lymphatic filariasis: the case for integrated vector management. *The Lancet infectious diseases*, 13(1):89–94, 2013.

[23] Paul van den Driessche and James Watmough. Reproduction numbers and sub-threshold endemic equilibria for compartmental models of disease transmission. *Mathematical Biosciences*, 180(1–2):29–48, 2002. doi: 10.1016/S0025-5564(02)00108-6.

[24] T. Waje, C. Iliyasu, L. M. Yaki, and I. K. Auta. A review of epidemiology of lymphatic filariasis in nigeria. *Pan African Medical Journal*, 2024. doi: 10.11604/pamj.2024.47.142.39746.

[25] World Health Organization. *Lymphatic filariasis*. World Health Organization, 2015.